International Journal of Biological Macromolecules 155 (2020) 543–550

Contents lists available at ScienceDirect

International Journal of Biological Macromolecules

journal homepage: http://www.elsevier.com/locate/ijbiomac

The status of the terminal regions of α-synuclein in different forms of aggregates during fibrillization

Amir Tayaranian Marvian [a,b,c], Farhang Aliakbari [a,d], Hossein Mohammad-Beigi [d], Zeinab Alsadat Ahmadi [a], Sina Mehrpooyan [a], Frederik Lermyte [e], Mahour Nasouti [a], Joanna F. Collingwood [e], Daniel E. Otzen [d], Dina Morshedi [a,*]

[a] Bioprocess Engineering Department, Institute of Industrial and Environmental Biotechnology, National Institute of Genetic Engineering and Biotechnology, Tehran, Iran
[b] Department of Neurology, School of Medicine, Technical University of Munich, Munich, Germany
[c] Department of Translational Neurodegeneration, German Center for Neurodegenerative Diseases (DZNE), Munich, Germany
[d] Interdisciplinary Nanoscience Centre (iNANO), Department of Molecular Biology and Genetics, Aarhus University, Gustav Wieds Vej 14, DK–8000 Aarhus C, Denmark
[e] School of Engineering, University of Warwick, Coventry, UK

ARTICLE INFO

Article history:
Received 3 February 2020
Received in revised form 26 March 2020
Accepted 27 March 2020
Available online 31 March 2020

Keywords:
Alpha-Synuclein
Fibrillization
Fluorescence
Oligomer
Protein terminal labeling

ABSTRACT

The α-synuclein (αSN) amyloid fibrillization process is known to be a crucial phenomenon associated with neuronal loss in various neurodegenerative diseases, most famously Parkinson's disease. The process involves different aggregated species and ultimately leads to formation of β-sheet rich fibrillar structures. Despite the essential role of αSN aggregation in the pathoetiology of various neurological disorders, the characteristics of various assemblies are not fully understood. Here, we established a fluorescence-based model for studying the end-parts of αSN to decipher the structural aspects of aggregates during the fibrillization. Our model proved highly sensitive to the events at the early stage of the fibrillization process, which are hardly detectable with routine techniques. Combining fluorescent and PAGE analysis, we found different oligomeric aggregates in the nucleation phase of fibrillization with different sensitivity to SDS and different structures based on αSN termini. Moreover, we found that these oligomers are highly dynamic: after reaching peak levels during fibrillization, they decline and eventually disappear, suggesting their transformation into other αSN aggregated species. These findings shed light on the structural features of various αSN aggregates and their dynamics in synucleinopathies.

1. Introduction

Amyloid fibrillization of α-synuclein (αSN) is a critical process in synucleinopathies such as Parkinson's disease (PD) [1]. Intraneuronal amyloid fibril deposits called Lewy inclusions are considered predominant hallmarks of PD, and are mainly constituted of αSN aggregates [2]. Studies to identify the toxic aggregated species of αSN have illustrated the role of fibrillar structures in the pathology [3], while a growing body of evidence highlights the destructive function of intermediate aggregates and oligomeric structures leading to neurodegeneration [4–6]. Consequently, the structural features and process of formation of these intermediate aggregates are under intense investigation.

αSN is a small 140-residue natively unfolded protein [7], which is found at a high concentration in the presynaptic region of neurons [8]. Traditionally, the αSN sequence is divided into three regions including: the membrane interacting N-terminus, the central region containing non-amyloid component sequence (NAC), and the acidic C-terminal region [9]. The highly flexible structure of αSN and presence of the aggregation-prone NAC domain provides high potential in this protein for self-aggregation and generation of fibrillar structures [9]. *In vitro* experiments on αSN fibrillization lead to a common sigmoidal fibrillization process which is divided into three major steps including: lag phase (or nucleation), exponential phase (or elongation), and plateau phase [10]. Gaining a clear overview of the fibrillization process, including the molecular conversions and structural features, will help the development of therapeutic approaches.

αSN fibrils are composed of β-strand structures, which are routinely studied with amyloid-reporter dyes, including the thioflavin family [11,12]. Despite their high efficiency, the thioflavin family is hardly capable of detecting the non-fibrillar intermediate aggregates because of their low concentration, transient nature, and also because of the uncertainty about their composition. As an alternative, fluorescent labeling of αSN protein with thiol- or amine-reactive dyes has been used to visualize aggregates independent of β-strand content *in vitro* and *in vivo*

* Corresponding author at: National Institute of Genetic Engineering and Biotechnology, Shahrak-e Pajoohesh, km 15 Tehran - Karaj Highway, P.O. Box:14965/161, Tehran, Iran.
E-mail address: morshedi@nigeb.ac.ir (D. Morshedi).

https://doi.org/10.1016/j.ijbiomac.2020.03.238

[13–16], since they monitor structural conversions based on reactivity towards these dyes which in turn depend on solvent exposure and intramolecular motion of the reactive amino acids.

Despite general agreement about the role of the αSN NAC domain in fibrillization [17], the role of its terminal regions in this process is still controversial. Tryptophan substitution and protease digestion studies suggested that the N- and C-termini of αSN are exposed in the fibril state [18–20]; however, site-specific fluorescent labeling showed some degree of interprotein interaction [21]. The debate about αSN oligomers is even more challenging: although toxicity was shown in various studies, the complete structure, variety and identity of these species are not precisely described [22]. Accordingly, investigating the roles of these termini in varied species of aggregates in order to understand the structures and conversions of species during the fibrillization process may be very helpful for the development of therapeutic strategies.

In the present study, we fluorescently labeled both terminal regions of αSN with minimal alteration to the natural properties of the protein, especially amyloid fibrillization. Different analyses including ThT, AFM, fluorescence imaging and anisotropy confirmed the labeling of the aggregated structures formed in the fibrillization process. Using this model, we analyzed fluorescence alterations, which reflect structural conversions during fibrillization. Basically, solvent exposure and mobility of a fluorescent probe can be altered *via* aggregation, which affects the traceable fluorescence features. Moreover, fluorescence changes in the primary stage of fibrillization were interpreted by monitoring oligomers in the fibrillization process with polyacrylamide gel electrophoresis (PAGE). Based on these data, we present an aggregation model including the αSN species identified in this study, and the proposed role of the termini in this process. These findings broaden the landscape concerning the characteristics of potentially pathogenic species in synucleinopathies and pave the way for the future analysis of intermediate proteinaceous aggregates.

2. Materials and methods

2.1. Materials

Escherichia coli BL21 (DE3) pLysS cells were from Novagen (Madison, WI, USA). mBBr was from Santa Cruz Biotechnology (sc-214629). Bicinchoninic acid (BCA) assay kit (BCA-1) was from Parstous Biotechnology. Thioflavin T (ThT), ethylenediaminetetraacetic acid (EDTA) and phenylmethane sulfonyl fluoride (PMSF) were from Sigma-Aldrich (St Louis, MO). All chemicals were of analytical grade from Merck (Germany).

2.2. Expression and purification of WT and mutated αSN

pNIC28-Bsa4 plasmids containing wild type or mutants αSN (N-terminal mutation: M5C, C-terminal mutation: G132C) were transformed in *E. coli* BL21 (DE3) pLysS cells. αSN was expressed and purified as described by Lorenzen et al. [23]. In brief, recombinant αSN was expressed in BL21 *E. coli* species and purified in three major steps including osmotic shock, anion-exchange and size exclusion chromatography. Protein concentration was determined by using bicinchoninic acid (BCA) assay kit. The purified protein was freeze-dried and stored at −20 °C.

2.3. Mass spectrometry (MS) experimental

αSN (10 μM) was dissolved in Milli-Q grade water supplemented with 15 mM ammonium acetate (Fisher Scientific, Loughborough, UK). The 12 Tesla solariX quadrupole/FTICR instrument (Bruker Daltonik GmbH, Bremen, Germany) equipped with an infinity cell was employed for MS experiments. Ions were introduced using nano-electrospray ionisation in positive ion mode and externally accumulated in a hexapole collision cell before being transferred to the ICR cell. Precursor ions were selected in the quadrupole, aimed at tandem MS experiments. For collision-induced dissociation (CID), a collision voltage of 13 V was applied. Data were analyzed using Bruker Compass DataAnalysis 4.1, and the SNAP algorithm was employed for monoisotopic fragment masses.

2.4. Fluorescent labeling using monobromobimane (mBBr)

Mutants αSN (M5C and G132C) were dissolved in phosphate buffer saline (PBS) pH 7.4 and mBBr was dissolved in 100% DMSO at the concentration of 40 mM. A mixture including 200 μM protein and 2 mM mBBr was made (1:10 M ratio) in PBS and incubated at 37 °C for 2 h. The unconjugated probes were separated from the labeled protein with a desalting column (GE Healthcare, NAP-5). Finally, the labeled protein was freeze-dried and stored at −20 °C.

2.5. The induction and assessment of αSN fibrillization

Fibrillization was induced by incubating the dissolved purified protein (1 mg/mL) in PBS pH 7.4 containing EDTA (0.1 mM) and PMSF (0.1 mM) at 37 °C with constant orbital shaking at 300 rpm with 3 mm glass beads (Merck, 104015) in 96-well plate non-treated dishes over a period of 40 h. To eliminate the preformed aggregates, the protein solution was spun down at 13000 rpm for 10 min before beginning the fibrillization process. The rate of amyloid fibril formation was estimated using ThT fluorescence measurement at defined intervals. For fibrillization of mBBr labeled mutant protein, 5% N-terminal fluorescence labeled αSN (N-αSN-F) or C-terminal fluorescence labeled αSN (C-αSN-F) was mixed with 95% WT αSN under the same fibrillization condition. The Finke-Watzky (F—W) two-step model [24] was fitted to the normalized ThT fibrillization data (Eq. (1)) to compare the fibrillization features of each labeled protein with the WT:

$$F(t) = \frac{1}{1 + e^{-\nu\,(t - t_{1/2})}} \tag{1}$$

where $t_{1/2}$ is the time required to produce half the total product and ν is the growth rate.

2.6. ThT and mBBr fluorescence assays

ThT fluorescence intensity was measured to analyze the fibrillization process of αSN using 12 μM ThT in 10 mM Tris buffer, pH 8.0. Fluorescence emission spectra were obtained with the excitation wavelength 440 nm and the emission spectra obtained over the range 450–550 nm. The excitation and emission slit widths were fixed at 5 and 10 nm, respectively. mBBr fluorescence emission spectra were obtained with the excitation wavelength 386 nm and the emission spectra obtained over the range 400–550 nm. The excitation and emission slit widths were fixed at 10 and 20 nm, respectively. The spectral center of mass (ν_g) [25], was used for calculating the maximum emission wavelength according to Eq. (2):

$$\nu_g = \frac{\sum \nu_i F_i}{\sum F_i} \tag{2}$$

where F_i is the emission at a wavelength ν_i, and the sum includes all wavelengths where $F_i > 0$. Fluorescence experiments were carried out on a Varian Cary Eclipse fluorescence spectrophotometer (Mulgrave, Australia) at room temperature.

2.7. Separation and quantization of the soluble and insoluble fractions during the fibrilization

At sampling time points during incubation, the fibrillization solution was centrifuged at 17,000g for 60 min in an Eppendorf microcentrifuge

to separate the insoluble fraction (Pellet fraction) from the supernatant (SUP fraction). The amount of protein in each fraction was estimated using a BCA protein concentration assay kit.

2.8. Gradient SDS-PAGE and native PAGE

Gradient SDS-PAGE of 4–16% was run in SDS-containing Tris-Glycine buffer (250 mM Tris, 200 mM Glycine, 1% SDS) with a constant current of 10 mA. Protein samples were added to 6× loading buffer (500 mM Tris-HCl pH 6.8, 50% Glycerol, 0.2% Bromophenol blue, 12% SDS) to obtain 1× buffer. For gradient (4–16%) native-PAGE, detergent-free versions of all solutions were used. 50 μg of protein was loaded into each well, and the protein bands were visualized *via* silver nitrate staining as described [26].

2.9. Statistical analysis

To test for statistically significant differences between averages, a one-way ANOVA with Tukey's *post hoc* test was conducted. Probability values <0.05 (indicated with *) were considered significant.

3. Results

3.1. Generation and characterization of fluorescently labeled αSN

Self-aggregating proteins such as αSN contain regions with a high tendency to self-assembly [19,27,28]. In this study, we prepared single-Cys mutants of αSN for residue-specific fluorescence labeling. Using the web-based AGGRESCAN server we identified Met5 and Gly132 as the suitable residues to replace with Cys without perturbing hot spot regions of aggregation (Fig. 1). Subsequent to expression and purification, M5C and G132C αSN were validated with mass spectrometry (Fig. S1A-G). As depicted from Fig. S1A and D, CID data for M5C show that modification is in the first 112 amino acid residues. Obviously we had to narrow it down more; therefore, ECD was used to fragment this protein as well. ECD (Fig. S1B and F) results show that the modification is in the first 14 N-terminal residues. Regarding the G132C however, CID (Fig. S1C and E) was sufficient to narrow down the modification site to [Pro128 – Gln134] making it very likely that this is indeed G132C. Moreover, a very good match for intact precursor mass makes it likely that the expression and modification worked as planned (Fig. S1G). In all cases, tandem MS was used for added confidence, and (for the mutants) narrowing down the region of the modification. The characteristics of N-terminal and C-terminal mutated proteins were also compared with wild-type (WT) by SDS-PAGE and Western blotting (Fig. S2A and B). Fluorescence imaging of SDS-PAGE bands following the mBBr labeling showed high fluorescence intensity of N-terminal (N-αSN-F) and C-terminal (C-αSN-F) fluorescently labeled mutants αSN, while the WT αSN did not show any mBBr fluorescence activity after exposure to label (Fig. S2C). The excitation and emission spectrum for N-αSN-F and C-αSN-F displayed well-defined mBBr monomeric peaks at 386 nm and 474 nm for excitation and emission, respectively (Fig. S2D) [29]. Circular dichroism (CD) spectrum analysis showed no differences between WT and labeled mutants αSN that represent similar secondary structures in the labeled monomeric mutants compared to WT (Fig. S2E).

3.2. Amyloid fibrillization features of N- and C-terminal labeled mutants αSN are almost identical to WT

To test the efficacy of our fluorescence model, the aggregation features of the labeled mutants αSN were studied using the ThT fluorescence assay (Fig. 2). Fitting with the Finke-Watzky model (Eq. (1)) revealed that the growth rate (ν) of the fibrillization in 5% labeled mutants was similar to WT. However, the half times ($t_{1/2}$) of the fibrillization were about 1 and 3 h longer than WT for N-αSN-F and C-αSN-F, respectively [24]. These data confirm that N-αSN-F and C-αSN-F caused some delay in the fibrillization; however, the qualitative profile of the process was comparable with WT.

Polarization assays are useful tools to monitor the aggregation of proteins, using either intrinsic Trp fluorescence or extrinsically added fluorophores. In the aggregated state, each molecule will rotate slower than in the monomeric state during the excited state lifetime [25]. αSN has no Trp residue but we were able to monitor the anisotropy of N-αSN-F and C-αSN-F to monitor αSN aggregation (Fig. 3A). Our data showed that the increase in mBBr anisotropy accompanies the progress of fibrillization for the mixture of 5% N-αSN-F or C-αSN-F with 95% of WT-αSN. This finding indicates that the fibrillization of αSN leads to a decrease in the label rotation in the aggregated state, which suggests the labeled αSN is associated with the aggregation process.

Both fluorescence microscopy (Fig. 3B) and atomic force microscopy (AFM) (Fig. 3C) revealed the same overall morphology for fibrils formed by WT αSN and the labeled proteins.

3.3. Finding the position of N- and C-terminal regions during αSN fibrillization

When Cys-bonded mBBr is transferred from water to DMSO, its fluorescence emission intensity increases 4–5 fold, and the peak position is blue-shifted from 474 to 453 nm (Fig. S3), which illustrate the high sensitivity of mBBr towards the hydrophobicity of its environment. We exploited this to monitor changes in the environment around residues 5 and 132 during the fibrillization. For N-αSN-F, mBBr intensity increases by ~20% after 7 h, with a further significant increase to ~ 30%

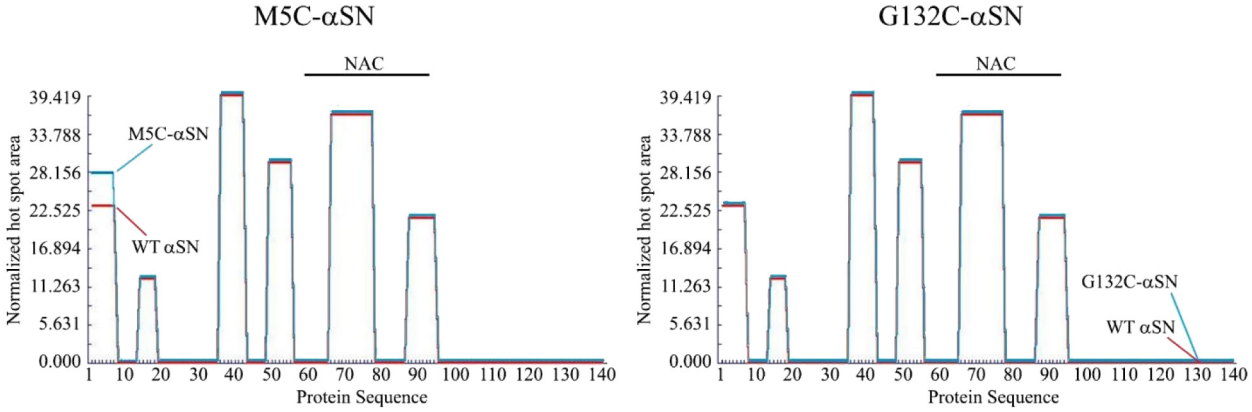

Fig. 1. The prediction of the impact of Cys mutations at positions 5 and 132 of αSN on aggregation hotspots. AGGRESCAN profile, comparing αSN wild-type hotspot pattern (red lines) for aggregation with M5C-αSN and G132C-αSN (blue lines). M5C-αSN (Left) showed a little difference in the first hotspot of aggregation at the N-terminus from the wild-type. The G132C-αSN hotspot pattern of aggregation (Right) shows no divergence from the wild-type pattern.

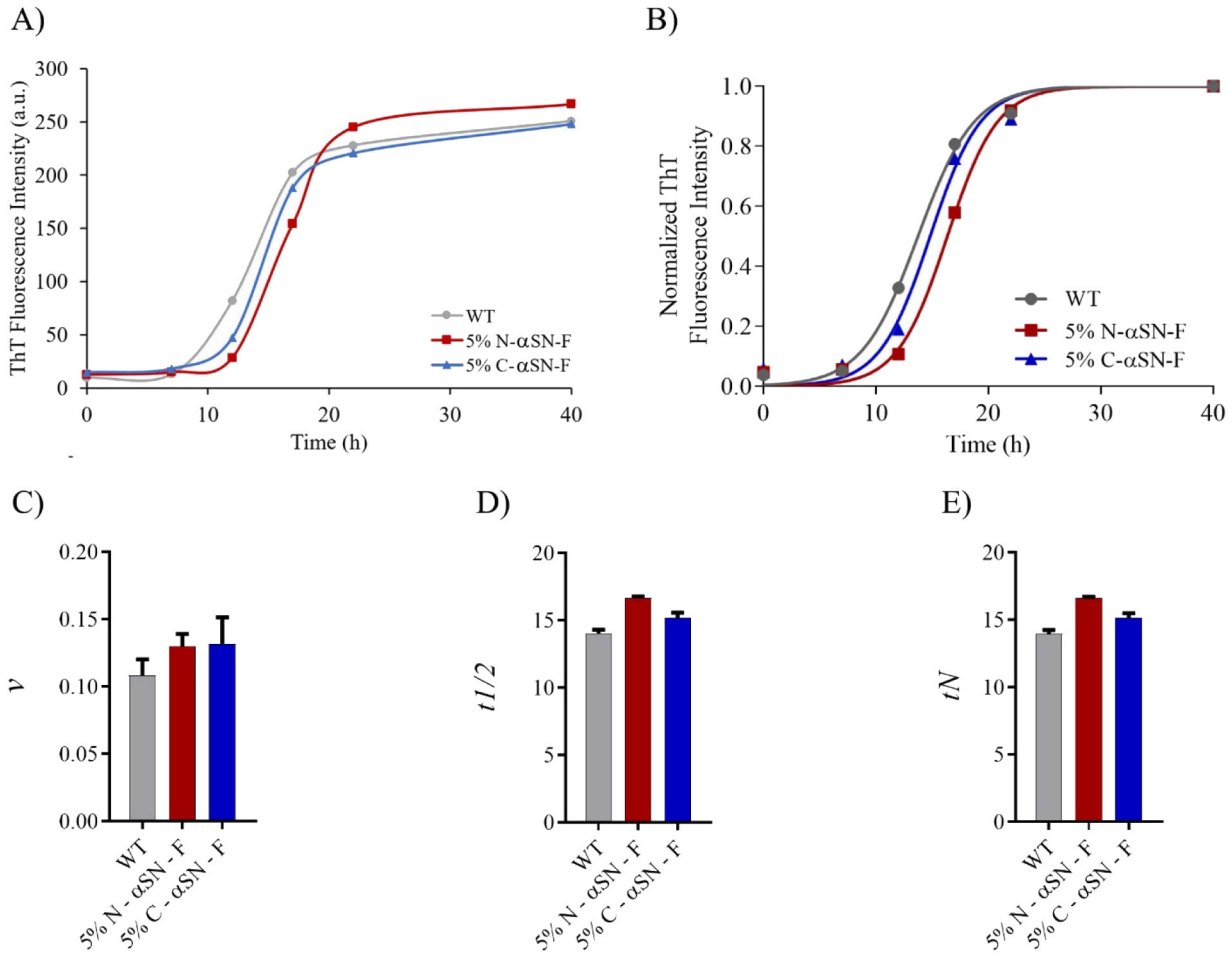

Fig. 2. Fibrillization kinetics of WT and the labeled mutants of αSN. A) ThT assays for the fibrillization of N-αSN-F and C-αSN-F and WT-αSN at 37 °C, pH 7.4. B) The Finke–Watzky model was fitted to the normalized outcomes of the ThT adopted from the aggregation kinetic of αSN in A. (C-E) Kinetic parameters based on Finke-Watzky equation for WT and labeled mutants αSN fibril formation, (C) growth rate: ν, (D) half time: $t1/2$, and (E) lag time: tN.

at 12 h (Fig. 4A). At the end of the exponential stage (24 h) of fibril formation, the mBBr intensity increase reached ~ 70%, and then decreased to 60% in the plateau phase of the fibrillization process. The emission center of mass for mBBr blue-shifted with a similar time profile to the fluorescence intensity graph, which further confirms the variation in the microenvironment during the fibrillization (Fig. 4B).

For C-αSN-F in the fibrillization condition, we observed a significant ~40% increase after 17 h of incubation (Fig. 4C). Beyond the plateau stage, the mBBr intensity finally reached steady-state at a value of ~25% higher than the plateau phase of the fibrillization. The emission center of mass further verified the results of the intensity analysis (Fig. 4D). The increase in the mBBr intensity and blue-shift in the emission spectral center of mass suggested the alteration of the probe microenvironment to the more hydrophobic area. These data suggest the differences in the behavior of αSN end-parts in the intermediate stages during the fibrillization process, in which N-αSN-F was more sensitive than C-αSN-F towards changes.

The ThT results show that ThT is insensitive to events in the nucleation phase of αSN fibrillization (up to 10 h of incubation). However, the N-αSN-F models were shown to be considerably sensitive to early molecular events. The mBBr fluorescence intensity of N-αSN-F showed a variation of up to 30% from the steady-state (Fig. 4A). This finding illustrates the high capability of these fluorescent models to monitor the early events of αSN amyloid aggregation.

Analyzing aggregated species of αSN during fibrillization by mBBr-labeling.

The presence of various soluble and insoluble aggregated species during the amyloid fibrillization process of αSN has been shown [10]; however, the order of events and the conversion between species is not understood clearly, especially in the nucleation phase. In order to obtain an overview of the molecular events under our experimental conditions, we separated the soluble and insoluble species after the aggregation process by using centrifugation (Fig. 5A). We found that the amount of protein in the insoluble fraction is directly related to the ThT level. Conversely, the protein concentration in the soluble fraction decreased gradually as the fibrillization process progressed. These results suggest that in the nucleation phase, soluble intermediate structures might be the causes of alteration in mBBr fluorescence.

To further decipher the intermediate structures in the nucleation phase, we used gradient PAGE analysis for tracing of the soluble oligomers. In order to have a complete perspective on the molecular events, we used denaturing and non-denaturing systems to trace the SDS-resistant and SDS-sensitive oligomeric species. According to the denaturing PAGE results, we found large oligomeric species (>245 kDa) which started to appear under fibrillization conditions after 4 h (in the nucleation phase) and were maximized in abundance at the exponential phase of the process (12 h) and then disappeared gradually at later times of incubation (Fig. 5B). Moreover, the non-denaturing PAGE revealed the presence of oligomeric species at the beginning point of the fibrillization process, which gradually disappeared in the lag phase of fibrillization (Fig. 5C). The absence of this intense band in the SDS-PAGE shows the high sensitivity of this species to denaturing

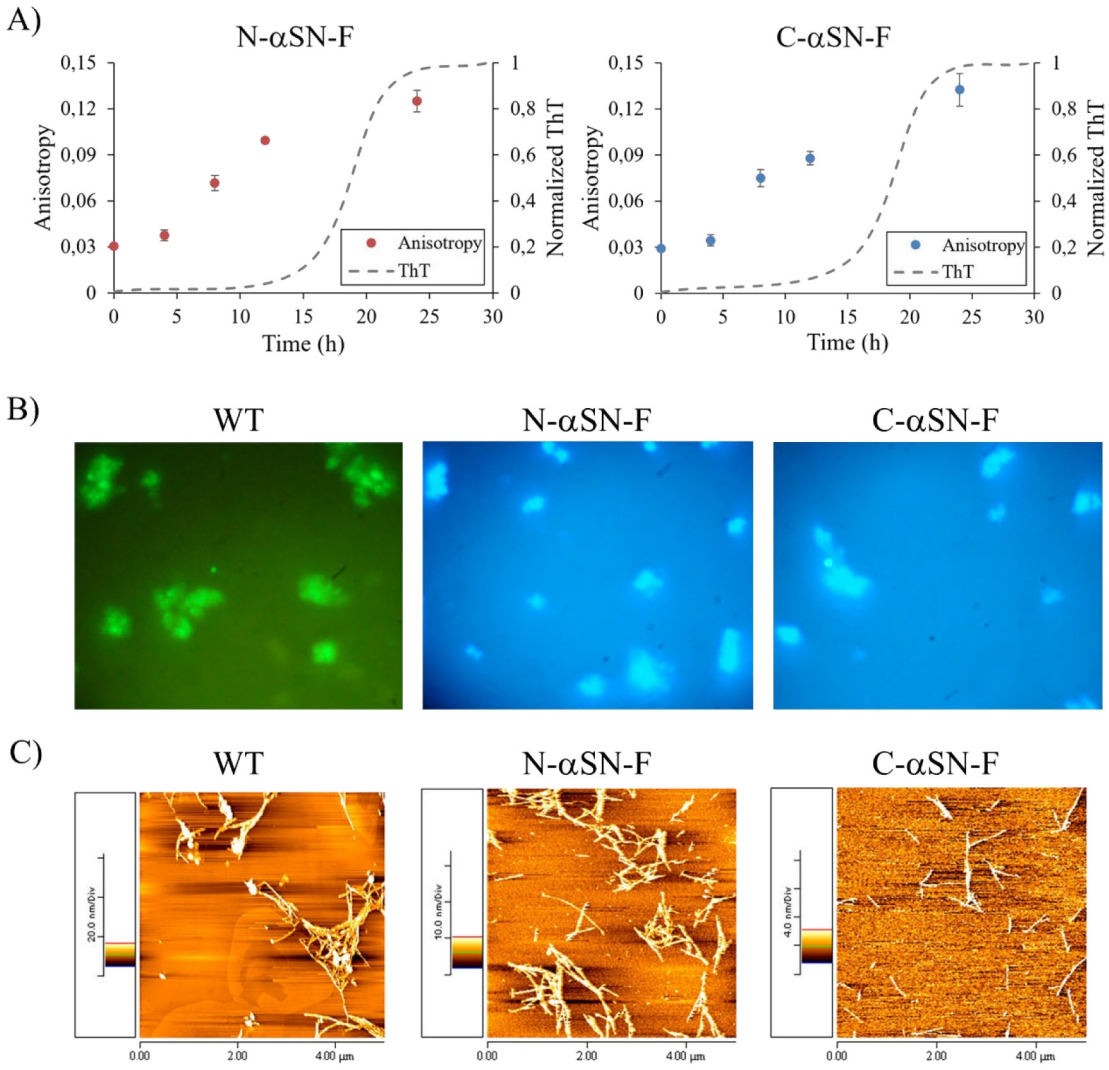

Fig. 3. Analysis of the fibrillization features of fluorescent-labeled αSN. A) Anisotropic study of the N-αSN —F (right) and C-αSN-F (left) shows the elevation of anisotropy during αSN fibrillization progresses in both protein models present at a proportion of 5% of total αSN. Fibrillization was carried out at 37 °C, and measurement was done at room temperature, pH 7.4. B) Fluorescence microscopy of the final fibrillar structure for WT (stained by ThT) and labeled proteins (fluorescence of mBBr) to compare the morphological features showing the similarity between aggregates. Magnification: 100×. C) AFM imaging of final fibrillar structures to compare the fibrillar structures which show similarity among the WT and the two labeled proteins.

treatment. Since having an accurate size calibration for the native-PAGE is a technical deficiency, the size of the oligomer band in this gel is not clear.

In the native-PAGE, the monomeric band disappeared gradually along with the progression of the fibrillization process because the intact fibrillar structures were incapable of penetrating into the gel. Conversely, as expected, in the SDS-PAGE the monomeric band intensity stays almost the same during the fibrillization, as the denaturing treatment unfolds the fibrillar structures. These data suggest that two different oligomer populations might be present in the αSN fibrillization with different biochemical properties over the different timeframes. This information on the lag phase of the fibrillization process paves the way for the interpretation of results from the mBBr fluorescence at the end-parts of αSN, which is discussed in the next section.

4. Discussion

Here we established and characterized a fluorescent model of αSN to analyze the status of fibril end-parts during the amyloid fibrillization process. We monitored the alteration in fluorescent features of the models during the fibrillization to infer the status of the end-parts. We showed that N-αSN-F model is highly sensitive to intermediate αSN aggregates, which are not easily detectable by other means. Furthermore, we categorized distinct aggregated species into three main fractions: monomers, oligomers and fibrils, to provide a structure for the interpretation of our fluorescence results at the molecular level.

The fluorescent models were generated by site-specific labeling of αSN at both end-parts using a thiol-reactive probe, mBBr, as described previously [30,31]. The small size of the mBBr fluorophore reduces the likelihood of changes in the natural biological, physical and chemical properties of the protein after labeling [32,33]. Moreover, the high sensitivity of mBBr to the polarity of its microenvironment makes it a great tool for monitoring the status of the end-parts of αSN during fibrillization [29]. The fluorescence and structural analysis revealed that both mutated forms of αSN, including N-terminal labeled (N-αSN-F) and C-terminal labeled (C-αSN-F) were efficiently probed and that they also show similar features as WT protein such as CD spectrum. Studying the fibrillization by ThT showed that the fibrillization kinetics for WT with the inclusion of 5% N-αSN-F or C-αSN-F are similar to those for 100% WT. Anisotropy analysis demonstrated the incorporation of the

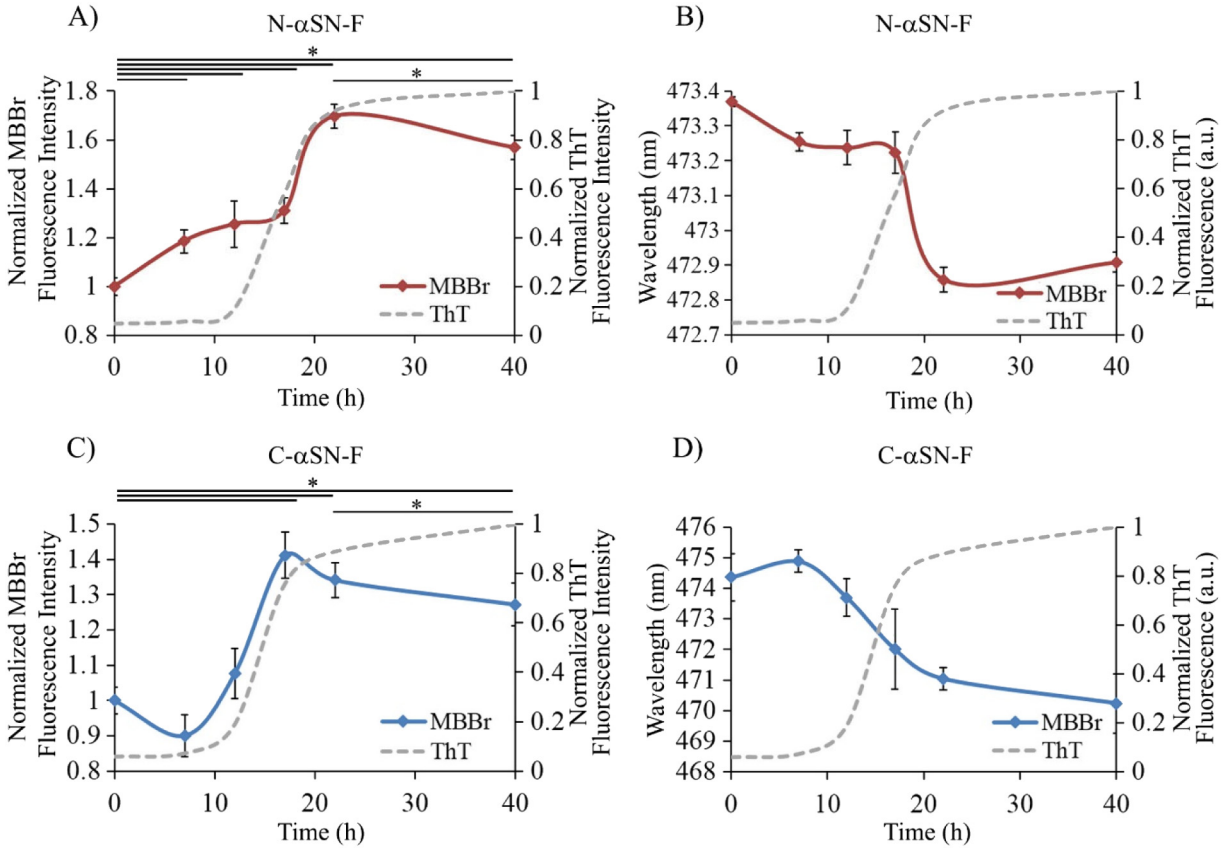

Fig. 4. MBBr fluorescence modulation during the fibrillization process. A) MBBr intensity change, and B) MBBr emission center of mass shifting, during the fibrillization of 5% N-αSN-F (red) along with ThT intensity (gray dashed line). C) MBBr intensity change, and D) MBBr emission center of mass shifting, during the fibrillization of 5% C-αSN-F (blue) along with ThT intensity (gray dash line). Fibrillization was carried out at 37 °C, and measurement was done at room temperature, pH 7.4. *$p < 0.05$ with a one-way ANOVA with Tukey's *post hoc* test. Error bars are represented as normalized SD.

5% labeled αSN in the final fibrillar aggregates, and AFM images demonstrated the resemblance of the ultimate fibrillar structures of WT to those incorporating labeled αSN.

Studying the protein concentration in soluble and insoluble fractions during the fibrillization revealed a gradual decrease in the soluble fraction and an increase in the insoluble fraction in accordance with the ThT emission profile, which confirms the progress of fibrillization. Monitoring N-αSN-F showed 20% to 30% increase in the lag phase of fibrillization from the monomeric baseline fluorescence intensity, which then increased to 60% - 70% in the plateau phase. This result was confirmed by a continuous blue-shift of the emission λ_{max}, which suggests that the N-terminus of αSN undergoes microenvironmental translocation into a more hydrophobic milieu. Combining this information with SDS-PAGE analysis revealed that in the absence of insoluble fibrillar structures in the lag phase (evidenced by lack of ThT signal and insoluble pellet), the increase in the mBBr fluorescence intensity might be related to the large SDS-resistant oligomeric species that were identified in this stage. The intermolecular contacts of the N-terminus with the NAC domain (residue 39–89) in the oligomeric species were reported previously [34], which may explain the mBBr behavior. Experimental studies and computational predictions have also confirmed the major role of the N-terminus in the primary phase of αSN self-aggregation [35–37].

Despite the presence of oligomers in the nucleation phase, ThT was completely insensitive to these species. Conversely, a 30% increase in the N-αSN-F fluorescence intensity illustrates the high sensitivity of this probe to the translocation of the N-terminal region of αSN oligomers (residue 5) into a more hydrophobic milieu. The significant reduction in the plateau phase of fibrillization from 70% to 60% in the N-αSN-F and 40% to 25% in C-αSN-F can be explained by the gradual disappearance of oligomers during the fibrillization process. Moreover, this observation suggests that in fibrillar structures, end-terminals are in less hydrophobic environment compare to oligomers.

The association of the N- and C-terminal regions (residue 7 and 136) in fibrillar structures was revealed by studying the microenvironment of these regions [21]. On the contrary, tryptophan substitution showed that these regions are not associated with fibrillization [14,18]. The later was further confirmed by protease digestion of αSN fibrils [20]. Our study suggests that both N and C-termini of αSN are located in a more hydrophobic area in fibrillary structure compared to the monomeric form. Despite reports of the unstructured (disordered) state of the N-terminus (residues 1–30) and C-terminus (residue 100–140) in fibrils, the interaction between protofilaments has been proved, explaining the microenvironmental changes at the end parts of αSN [38–40].

Despite solvent exposure altering the fluorescence behavior of the probe, the aggregation itself is also a possible mechanism for this phenomenon *via* aggregation induction emission (AIE) [41]. In AIE, restriction of intramolecular motions caused by aggregation can change the fluorescence behavior of a probe. Blue-shift and elevation of intensity in fibrils can arise due to the more compact nature, or interaction, of end-parts. This results in AIE, as there is a less intramolecular motion for mBBr in those regions compared to free monomers, which is also showed by anisotropy. The same interpretation should be considered for the fluorescence alteration in oligomers as well. More accurate structural studies utilizing methods such as NMR and cryo-EM are required to find the exact role of AIE and solvent accessibility in altering the fluorescence of end-parts in each aggregated species.

The recent kinetic model for αSN fibrillization described two oligomeric types which convert in a stepwise process leading finally to the

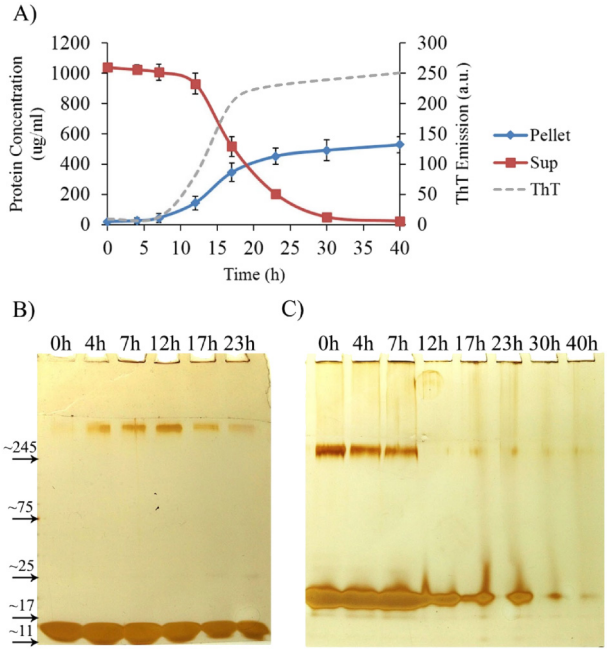

Fig. 5. Studying the different species of aggregates during the αSN fibrillization process. A) BCA protein concentration analysis for soluble (red) and insoluble (blue) fractions during the fibrillization process. ThT is shown as a gray dashed line. Measurement was done at room temperature, pH 7.4. B) Gradient SDS-PAGE (4–16%) analysis of samples from different incubation times during the fibrillization process. Monomers were observed below the 17 kD band and oligomers were observed above the 245 kD band of protein ladder. C) Gradient native-PAGE (4–16%) analysis of samples from different incubation times during the fibrillization process. Gels were developed using the silver staining method.

formation of fibrils [42]. They suggested that both types of oligomers are kinetically stable and are present until the end of the fibrillization process. However, our results showed that the oligomers we detected by PAGE analysis were highly dynamic, and vanished during the fibrillization. Our findings support the previous model proposed by Fink (2006) [10].

Taken together, our findings demonstrate that mBBr labeling of αSN at the end-parts is a highly sensitive method for monitoring the events in the nucleation phase of fibrillization, especially the N-terminal labeling. Our interpretation of the fluorescence data based on the fractionation and characterization of the fibrillization soup revealed the status of αSN termini in different aggregates during various phases of fibrillization. Our findings provide a more comprehensive perspective on the molecular events occurring during the fibrillization of αSN, in which the intermediate structures are better defined. These results enhance our understanding of the biochemical features of this pathophysiological phenomenon and pave the way for future investigations of the role of aggregated species in αSN pathogenesis.

Declaration of competing interest

The authors declare that they have no known competing financial interests or personal relationships that could have appeared to influence the work reported in this paper.

Acknowledgments

This work was mainly supported by the National Institute of Genetic Engineering and Biotechnology (NIGEB, Grant nr. 990201-I-751), Tehran, Iran, to D.M. and in part by the Engineering and Physical Sciences Research Council (EPSRC), UK, to J.F.C. (Grant nr. EP/N033191/1).

Appendix A. Supplementary data

Supplementary data for this article can be found online at https://doi.org/10.1016/j.ijbiomac.2020.03.238, and the spectral data will be accessible via the University of Warwick open access research repository (WRAP) at https://wrap.warwick.ac.uk/135091.

References

[1] C.M. Dobson, Protein folding and misfolding, Nature 426 (2003) 884–890.
[2] C.W. Shults, Lewy bodies, Proc. Natl. Acad. Sci. U. S. A. 103 (2006) 1661–1668.
[3] T.M. Dawson, V.L. Dawson, Molecular pathways of neurodegeneration in Parkinson's disease, Science. 302 (2003) 819–822.
[4] H.A. Lashuel, B.M. Petre, J. Wall, M. Simon, R.J. Nowak, T. Walz, P.T. Lansbury Jr., Alpha-synuclein, especially the Parkinson's disease-associated mutants, forms pore-like annular and tubular protofibrils, J. Mol. Biol. 322 (2002) 1089–1102.
[5] N. Reixach, S. Deechongkit, X. Jiang, J.W. Kelly, J.N. Buxbaum, Tissue damage in the amyloidoses: transthyretin monomers and nonnative oligomers are the major cytotoxic species in tissue culture, Proc. Natl. Acad. Sci. U. S. A. 101 (2004) 2817–2822.
[6] C. Williams-Gray, Seeing is believing: alpha-synuclein oligomers in Parkinson's disease brain, Mov. Disord. 30 (2015) 1324-1324.
[7] K.A. Conway, J.D. Harper, P.T. Lansbury, Accelerated in vitro fibril formation by a mutant alpha-synuclein linked to early-onset Parkinson disease, Nat. Med. 4 (1998) 1318–1320.
[8] L.S. Forno, Neuropathology of Parkinson's disease, J. Neuropathol. Exp. Neurol. 55 (1996) 259–272.
[9] V.N. Uversky, Neuropathology, biochemistry, and biophysics of alpha-synuclein aggregation, J. Neurochem. 103 (2007) 17–37.
[10] A.L. Fink, The aggregation and fibrillation of alpha-synuclein, Acc. Chem. Res. 39 (2006) 628–634.
[11] H. LeVine 3rd, Quantification of beta-sheet amyloid fibril structures with thioflavin T, Methods Enzymol. 309 (1999) 274–284.
[12] D. Stiller, D. Katenkamp, Fluorescence optical demonstration of amyloid by means of thioflavin S, Zentralbl Allg Pathol. 113 (1970) 451–465.
[13] P.J. McLean, H. Kawamata, B.T. Hyman, Alpha-synuclein-enhanced green fluorescent protein fusion proteins form proteasome sensitive inclusions in primary neurons, Neuroscience 104 (2001) 901–912.
[14] A. Dusa, J. Kaylor, S. Edridge, N. Bodner, D.P. Hong, A.L. Fink, Characterization of oligomers during alpha-synuclein aggregation using intrinsic tryptophan fluorescence, Biochemistry. 45 (2006) 2752–2760.
[15] M.J. Roberti, C.W. Bertoncini, R. Klement, E.A. Jares-Erijman, T.M. Jovin, Fluorescence imaging of amyloid formation in living cells by a functional, tetracysteine-tagged alpha-synuclein, Nat. Methods 4 (2007) 345–351.
[16] T.J. van Ham, A. Esposito, J.R. Kumita, S.T. Hsu, G.S. Kaminski Schierle, C.F. Kaminski, C.M. Dobson, E.A. Nollen, C.W. Bertoncini, Towards multiparametric fluorescent imaging of amyloid formation: studies of a YFP model of alpha-synuclein aggregation, J. Mol. Biol. 395 (2010) 627–642.
[17] H. Miake, H. Mizusawa, T. Iwatsubo, M. Hasegawa, Biochemical characterization of the core structure of alpha-synuclein filaments, J. Biol. Chem. 277 (2002) 19213–19219.
[18] J. Kaylor, N. Bodner, S. Edridge, G. Yamin, D.P. Hong, A.L. Fink, Characterization of oligomeric intermediates in alpha-synuclein fibrillation: FRET studies of Y125W/Y133F/Y136F alpha-synuclein, J. Mol. Biol. 353 (2005) 357–372.
[19] F. Chiti, C.M. Dobson, Protein misfolding, functional amyloid, and human disease, Annu. Rev. Biochem. 75 (2006) 333–366.
[20] Z. Qin, D. Hu, S. Han, D.P. Hong, A.L. Fink, Role of different regions of alpha-synuclein in the assembly of fibrils, Biochemistry 46 (2007) 13322–13330.
[21] T.L. Yap, C.M. Pfefferkorn, J.C. Lee, Residue-specific fluorescent probes of alpha-synuclein: detection of early events at the N- and C-termini during fibril assembly, Biochemistry 50 (2011) 1963–1965.
[22] N. Bengoa-Vergniory, R.F. Roberts, R. Wade-Martins, J. Alegre-Abarrategui, Alpha-synuclein oligomers: a new hope, Acta Neuropathol. 134 (2017) 819–838.
[23] N. Lorenzen, L. Lemminger, J.N. Pedersen, S.B. Nielsen, D.E. Otzen, The N-terminus of alpha-synuclein is essential for both monomeric and oligomeric interactions with membranes, FEBS Lett. 588 (2014) 497–502.
[24] A.M. Morris, M.A. Watzky, J.N. Agar, R.G. Finke, Fitting neurological protein aggregation kinetic data via a 2-step, minimal/"Ockham's razor" model: the Finke-Watzky mechanism of nucleation followed by autocatalytic surface growth, Biochemistry 47 (2008) 2413–2427.
[25] D.M.A. Jameson, Introduction to Fluorescence, CRC Press, 2014.
[26] R.C. Switzer 3rd, C.R. Merril, S. Shifrin, A highly sensitive silver stain for detecting proteins and peptides in polyacrylamide gels, Anal. Biochem. 98 (1979) 231–237.
[27] M.I. Ivanova, M.R. Sawaya, M. Gingery, A. Attinger, D. Eisenberg, An amyloid-forming segment of beta2-microglobulin suggests a molecular model for the fibril, Proc. Natl. Acad. Sci. U. S. A. 101 (2004) 10584–10589.
[28] S. Ventura, J. Zurdo, S. Narayanan, M. Parreno, R. Mangues, B. Reif, F. Chiti, E. Giannoni, C.M. Dobson, F.X. Aviles, L. Serrano, Short amino acid stretches can mediate amyloid formation in globular proteins: the Src homology 3 (SH3) case, Proc. Natl. Acad. Sci. U. S. A. 101 (2004) 7258–7263.
[29] S.E. Mansoor, H.S. McHaourab, D.L. Farrens, Determination of protein secondary structure and solvent accessibility using site-directed fluorescence labeling. Studies of T4 lysozyme using the fluorescent probe monobromobimane, Biochemistry 38 (1999) 16383–16393.

[30] J.W. Taraska, W.N. Zagotta, Fluorescence applications in molecular neurobiology, Neuron 66 (2010) 170–189.
[31] Y. Kim, S.O. Ho, N.R. Gassman, Y. Korlann, E.V. Landorf, F.R. Collart, S. Weiss, Efficient site-specific labeling of proteins via cysteines, Bioconjug. Chem. 19 (2008) 786–791.
[32] N.S. Kosower, E.M. Kosower, Thiol labeling with bromobimanes, Methods Enzymol. 143 (1987) 76–84.
[33] E.M. Kosower, N.S. Kosower, Bromobimane probes for thiols, Methods Enzymol. 251 (1995) 133–148.
[34] J.I. Gallea, M.S. Celej, Structural insights into amyloid oligomers of the Parkinson disease-related protein alpha-synuclein, J. Biol. Chem. 289 (2014) 26733–26742.
[35] H.J. Koo, H.J. Lee, H. Im, Sequence determinants regulating fibrillation of human alpha-synuclein, Biochem. Biophys. Res. Commun. 368 (2008) 772–778.
[36] N. Sanchez de Groot, I. Pallares, F.X. Aviles, J. Vendrell, S. Ventura, Prediction of "hot spots" of aggregation in disease-linked polypeptides, BMC Struct. Biol. 5 (2005) 18.
[37] S. Zibaee, R. Jakes, G. Fraser, L.C. Serpell, R.A. Crowther, M. Goedert, Sequence determinants for amyloid fibrillogenesis of human alpha-synuclein, J. Mol. Biol. 374 (2007) 454–464.
[38] M. Vilar, H.T. Chou, T. Luhrs, S.K. Maji, D. Riek-Loher, R. Verel, G. Manning, H. Stahlberg, R. Riek, The fold of alpha-synuclein fibrils, Proc. Natl. Acad. Sci. U. S. A. 105 (2008) 8637–8642.
[39] T. Guilliams, F. El-Turk, A.K. Buell, E.M. O'Day, F.A. Aprile, E.K. Esbjorner, M. Vendruscolo, N. Cremades, E. Pardon, L. Wyns, M.E. Welland, J. Steyaert, J. Christodoulou, C.M. Dobson, E. De Genst, Nanobodies raised against monomeric alpha-synuclein distinguish between fibrils at different maturation stages, J. Mol. Biol. 425 (2013) 2397–2411.
[40] K.A. Conway, J.D. Harper, P.T. Lansbury Jr., Fibrils formed in vitro from alpha-synuclein and two mutant forms linked to Parkinson's disease are typical amyloid, Biochemistry 39 (2000) 2552–2563.
[41] J. Mei, Y. Hong, J.W. Lam, A. Qin, Y. Tang, B.Z. Tang, Aggregation-induced emission: the whole is more brilliant than the parts, Adv. Mater. 26 (2014) 5429–5479.
[42] M. Iljina, G.A. Garcia, M.H. Horrocks, L. Tosatto, M.L. Choi, K.A. Ganzinger, A.Y. Abramov, S. Gandhi, N.W. Wood, N. Cremades, C.M. Dobson, T.P. Knowles, D. Klenerman, Kinetic model of the aggregation of alpha-synuclein provides insights into prion-like spreading, Proc. Natl. Acad. Sci. U. S. A. 113 (2016) E1206–E1215.